

On the physical structure, modelling and computation-based prediction of two-dimensional, smooth-wall turbulent boundary layers subjected to streamwise pressure gradients

Klewicki Joseph, Sandberg Richard, Knopp Tobias, Devenport William, Fritsch Daniel, Vishwanathan Vidya, Volino Ralph, Toxopeus Serge, McKeon Beverley & Eca Luis

To cite this article: Klewicki Joseph, Sandberg Richard, Knopp Tobias, Devenport William, Fritsch Daniel, Vishwanathan Vidya, Volino Ralph, Toxopeus Serge, McKeon Beverley & Eca Luis (19 Aug 2024): On the physical structure, modelling and computation-based prediction of two-dimensional, smooth-wall turbulent boundary layers subjected to streamwise pressure gradients, Journal of Turbulence, DOI: [10.1080/14685248.2024.2392572](https://doi.org/10.1080/14685248.2024.2392572)

To link to this article: <https://doi.org/10.1080/14685248.2024.2392572>



© 2024 The Author(s). Published by Informa UK Limited, trading as Taylor & Francis Group.



Published online: 19 Aug 2024.



Submit your article to this journal [↗](#)



Article views: 129




View related articles [↗](#)



View Crossmark data [↗](#)

On the physical structure, modelling and computation-based prediction of two-dimensional, smooth-wall turbulent boundary layers subjected to streamwise pressure gradients

Klewicki Joseph^a, Sandberg Richard^a, Knopp Tobias^b, Devenport William^c, Fritsch Daniel^c, Vishwanathan Vidya^c, Volino Ralph ^d, Toxopeus Serge^e, McKeon Beverley^f and Eca Luis^g

^aUniversity of Melbourne, Melbourne, Australia; ^bDeutsches Zentrum für Luft- und Raumfahrt e.V., Berlin, Germany; ^cVirginia Tech, Blacksburg, VA, United States; ^dUnited States Naval Academy, Annapolis, MD, United States; ^eMarine Research Institute Netherlands (MARIN), Wageningen, The Netherlands; ^fStanford University, Stanford, CA, United States; ^gInstituto Superior Tecnico, Lisbon, Portugal

ABSTRACT

This paper reports on the recent NATO Advanced Vehicle Technology (AVT) effort associated with smooth-wall two-dimensional turbulent boundary layer flows subjected to streamwise pressure gradients. The effort considered experiments, Reynolds Averaged Navier-Stokes (RANS) simulations, modelling, scaling and flow physics relative to the subject flows. Special attention is given to the current predictive capabilities and deficiencies of RANS simulations, and the interplay between experiments and RANS validation and development. In addition, the efficacy of the prediction of velocity field response and wall pressure statistics are respectively demonstrated via Resolvent and Gene Expression Programming based models. The persistence of a logarithmic mean velocity profile is evaluated and measures of non-equilibrium are described and discussed. A number of open issues are described and recommendations for future research are suggested.

ARTICLE HISTORY

Received 12 May 2024
Accepted 9 August 2024

KEYWORD

Pressure gradient turbulent boundary layers

1. Introduction

Owing to their technological relevance, there is on-going interest in better understanding and predicting non-canonical turbulent boundary layer flows. Here, non-canonical refers to flows that deviate from those that develop along smooth flat surfaces, and it is often the case that the given deviation is realised by subjecting the canonical flow to additional forces and/or through modifying boundary conditions. Under such effects, the boundary layer can be driven to what is generically referred to as a non-equilibrium state. Owing to the range of complexities introduced, both analytical approaches and numerical simulation strategies for non-equilibrium flows often face considerable challenges and open questions. Indeed, even a precise and universally agreed upon definition of non-equilibrium remains somewhat unresolved. Given this, we pragmatically adopt the definition of equilibrium employed in the recent review by Devenport and Lowe [1] as it provides a useful point of reference. Under this characterisation, equilibrium flows are self-preserving and thus the various statistical profiles admit an invariant representation under normalisations that properly employ locally defined characteristic length, time and velocity scales. Here we note, however, that according to this definition, the canonical zero pressure gradient flow is only in approximate equilibrium, as its equations do not admit a fully self-preserving form. Regardless, the definition of Devenport and Lowe constructively highlights scaling across parameter variations as a central challenge.

In this study we report on the work of the NATO AVT-349 subgroup on two-dimensional smooth-wall turbulent boundary layers subjected to pressure gradients in the stream direction. Central aims here are to describe the key findings of the AVT-349 effort and provide perspectives regarding the ramifications of these findings. This includes an articulation of the resulting open and/or unresolved issues associated with pressure gradient boundary layers. Toward these aims, we first describe the relevant experiments and computations conducted by the AVT-349 team and summarise the primary empirical findings. This includes commentary

CONTACT Klewicki Joseph  klewicki@unimelb.edu.au

© 2024 The Author(s). Published by Informa UK Limited, trading as Taylor & Francis Group.

This is an Open Access article distributed under the terms of the Creative Commons Attribution-NonCommercial-NoDerivatives License (<http://creativecommons.org/licenses/by-nc-nd/4.0/>), which permits non-commercial re-use, distribution, and reproduction in any medium, provided the original work is properly cited, and is not altered, transformed, or built upon in any way. The terms on which this article has been published allow the posting of the Accepted Manuscript in a repository by the author(s) or with their consent.

Table 1. Summary of key parameters associated with the smooth-wall pressure gradient experiments.

Study	$Re\tau$ range	β range	Sensors	Source publications
Virginia Tech	4000–11,000	−0.8 to 0.8	Pitot tubes, 2D2C PIV, surface microphones	[6,15,16]
UNH	7000–9800	0.0 to 1.9	3 wire hotwire probe	[18]
USNA	260–1900	−1.2 to 6.6	2 component LDV, 2D2C PIV	[20,21]
DLR/UniBw	6600–13,500	−1.7 to 46	2D3C, 3D3C PIV/PTV, OFI	[22,23]

Table 2. Summary of key parameters associated with the smooth-wall pressure gradient simulations.

Experiment	$Re\tau$ range	β range	Computers	Simulation type	Publications
Virginia Tech.	3400–5300	−1.0 to 1.0	Virginia Tech MARIN/IST, DLR Melbourne	2D and 3D RANS, 2D RANS 2D GEP RANS	[17,24] [26] [24,25]
DLR/UniBw 1	6600–9000	−1.7 to 47.	DLR	2D and 3D RANS	[23,37]
DLR/UniBw 2	8800–13,500	−1.7 to 46.	DLR	2D RANS	[23,37]
Virg. Tech. (ship scale Re)	$0.7\text{--}1.3 \times 10^6$	−1.0 to 1.0	MARIN/IST, DLR	2D	[26,49]

on the efficacy of the simulation methodology for the given problem. A series of sections are then presented that identify broader findings and/or important open questions. These are respectively associated with flow history effects, the existence/resilience of the logarithmic mean velocity profile, and the factors that need to be considered to obtain accurate Reynolds Averaged Navier-Stokes Simulations (RANS). Within each of these subsections, conclusions and/or supported positions are developed that incorporate the most significant findings. Broadly, these findings either point to specific conclusions, identify open questions or hypotheses requiring further scrutiny, or reveal the need for additional research.

2. Summary and observations of experiments and computations

This section first summarises the experimental studies and the complementary simulations conducted. Here, central questions pertain to the capacity of RANS to faithfully capture flow development. Connected to this is the capacity of the experiments to accurately mimic the idealisations employed in the simulation (e.g. 2D flow), or equivalently, the level of documentation about the experiments needed as inputs to properly simulate the intended flow field. Some modelling techniques with potential to address history effects in the flow are outlined, then a brief exposition of key observations from the experiments and simulations is then given.

2.1. Summary of studies

2.1.1. Physical experiments

Attributes of the four experiments conducted are given in Table 1. The following narrative provides additional details and context regarding these experiments. As can be seen, The Virginia Tech, University of New Hampshire (UNH) and University der Bundeswehr Mu"nchen (UniBw) experiments are at distinctively large Reynolds numbers, while the US Naval Academy (USNA) and Virginia Tech experiments cover an unusually broad range of pressure gradient conditions. In Tables 1 and 2 and throughout, the friction Reynolds number is given by $Re\tau = u_\tau \delta / \nu$, where, u_τ is the friction velocity ($= \sqrt{\tau_w / \rho}$ is the mean wall shear stress and ρ is the mass density), δ is the boundary layer thickness, ν is the kinematic viscosity, $\beta = \beta(x)$ is the Clauser pressure gradient parameter [2], $= (\delta_1 / \tau_w) dP/dx$, and $\delta_1 = \delta^*$ is the displacement thickness. The boundary layers described herein develop in the x direction with the wall normal direction denoted by y . The velocities in these directions are given by variants of u and v , with upper case or angle brackets signifying mean quantities. Researchers interested in gaining access to the data sets described herein are encouraged to contact the relevant authors directly.

A depiction of the Virginia Tech experiment is given in Figure 1. As shown, this experiment involved the application of favourable and adverse pressure gradients (FPG and APG, respectively) along a flat wall through pitching a symmetric airfoil in the freestream. In addition to a 3D laser scanned dimensional specification of the experiment geometry, these experiments involved mean static pressure measurements in the contraction, along the tunnel walls and along the airfoil surface. Mean velocity and turbulence measurements were acquired through the use of a Pitot-static boundary layer rake, 2D-3C PIV, and surface mounted microphones.

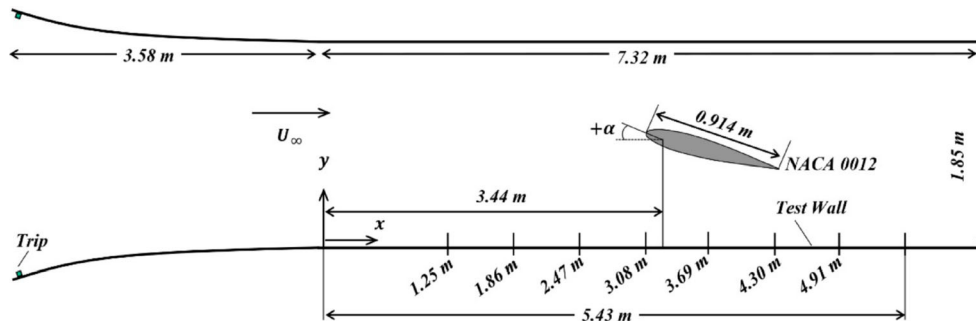


Figure 1. Schematic depiction of the Virginia Tech experiment configuration.

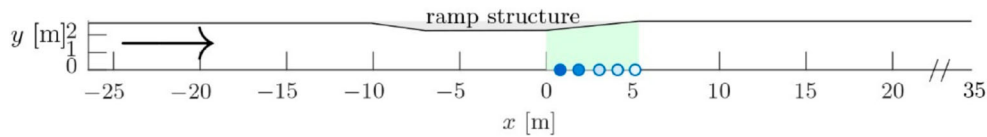


Figure 2. Schematic depiction of the University of New Hampshire experiment configuration. The shaded region locates the adverse pressure gradient region and markers denote measurement locations.

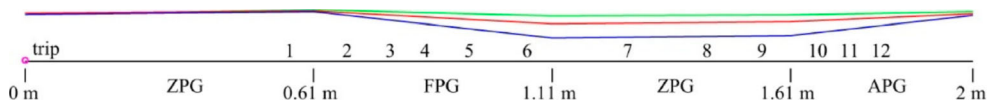


Figure 3. Schematic depiction of the streamwise pressure gradient experiment configurations in the US Naval Academy water channel.

Features of the UNH experiment are shown in Figure 2. In these experiments the pressure gradients were produced using a large ramp insert along the upper wall of the test section. The primary focus was on measurements in the APG region, although measurements were also acquired upstream and well-downstream of the ramp. The boundary layers studied developed along the lower wall. In addition to hotwire measurements of the mean and fluctuating streamwise (u) and wall-normal (v) velocities, these experiments employed Pitot-static probes to quantify the upstream flow conditions, freestream velocity, and the pressure variations in x .

The experiments at the USNA were conducted in a water channel along the flat surface beneath each of three ceiling ramp configurations as shown in Figure 3. The indicated variation in ramp angles provided for the relatively large range of β values listed in Table 1. An extensive set of well-resolved two component (u and v) Laser Doppler Velocimetry (LDV) measurements were acquired at stations 1-12. Planar (2D2C) PIV measurements were subsequently acquired over the same domain for all three ramp configurations.

Key elements of the DLR/UniBw experiments performed in the Eiffel-type atmospheric wind tunnel at University der Bundeswehr München are shown Figure 4. Like the UNH and USNA experiments, this experiment employed a ramp insert to produce a FPG, ZPG, APG sequence of pressure gradients. In this case, however, the measurements were acquired along the ramp surface to achieve strong APGs of $\beta > 20$ and thus also included the associated streamline curvature effects. Some of the large field-of-view PIV configurations are depicted in Figure 4. High-resolution particle tracking methods (PTV), such as microscopic PTV and Lagrangian PTV, were used in the APG region. In these experiments, measurements were also conducted to quantify the inflow profiles and the influence of the side walls.

2.1.2. Numerical simulations

Table 2 presents attributes of the RANS based computations that simulated the Virginia Tech and UniBw experiments listed in Table 1. Important aims of these simulations are to determine the degree to which RANS

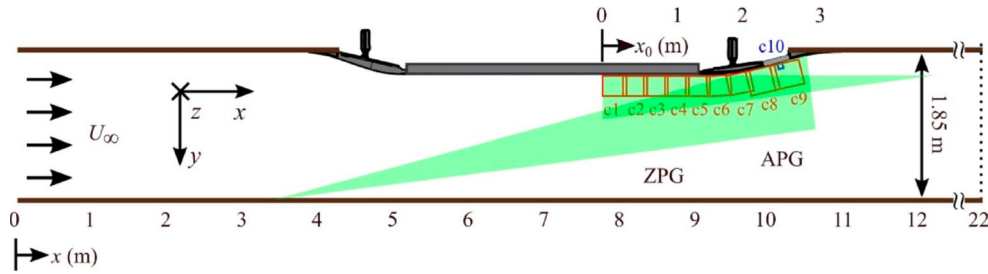


Figure 4. Schematic depiction of the joint DLR and University der Bundeswehr Muenchen experiment configuration.

calculations are able to faithfully predict 2D turbulent boundary layers over smooth walls when subjected to streamwise pressure gradients, and to clarify which factors underlie a failure to produce agreement between the measurements and simulations.

The Virginia Tech simulations implemented both 2D and 3D RANS. Both the 2D and 3D simulations used fully structured grids. The 2D case used a flat no-slip wall for the boundary layer development with an inflow length that was set to match the inflow Reynolds number. A slip wall was employed on the opposing wall. This boundary was angled to set the applied pressure gradient. Five levels of grid refinement were tested for the 2D simulations, with the final case having $N = 198,108$ grid cells. The 3D simulations employed a constant cross-section domain with no-slip boundaries.

The DLR/UniBw entries in Table 2 pertain to simulations of the DLR/UniBw experiments 1 and 2 listed in Table 1. Here, the grids were generated at DLR and a range of parameters affecting the simulation performance were explored. One set of experiments having an inlet freestream velocity of 23 m/s ($6600 < Re_\tau < 9500$, $-1.7 < \beta < 47$) investigated use of the Spalart and Allmaras model (SA) [3], the SST model [4] and the SSG/LRR- ω model [5], and employed an enlarged inflow length upstream of the pressure gradient ramp to ensure that the simulation attained the same δ_* and Re_{δ_*} value as in the experiment. The second DLR/UniBw entry in Table 2 uses the same inflow δ matching procedure, turbulence models and β range as the first, but had the inflow U_∞ set at 36 m/s and covers the Reynolds number range $8800 < Re_\tau < 13500$.

Additionally, DLR contributed as a computer to the simulations of the Virginia Tech experiments listed in Table 1. These are 2D simulations, and thus adjusted the upper slip wall to set the pressure gradient. The grid configuration was the same as that used by Fritsch et al. [6].

The MARIN/IST simulations listed in Table 2 were performed at Reynolds numbers comparable to the Virginia Tech experiments, but also at much larger Re_τ . Like the other 2D RANS simulations, these used an inviscid upper boundary that is tilted to match the pressure gradient in the experiment. The simulations used six turbulence models at both Reynolds numbers. These include five eddy-viscosity models: the one-equation SA model [3]; two versions of the two-equation, Shear-Stress Transport $k - \omega$ (SST) model proposed by Mentor et al. [4,7] the two-equation Turbulent Non-Turbulent $k - \omega$ (TNT) model of Kok [8] and the two-equation $k - \sqrt{kL}$ (KSKL) model described in [9]. The sixth model is the SSG/LRR- ω Reynolds-Stress model (RSM) proposed in [5].

To specifically address the issue of improving prediction accuracy using RANS, the Melbourne simulations of Table 2 employed a machine-learning strategy to optimise the turbulence model. It should be noticed that the model optimisation focused on overcoming the limitations of the Boussinesq hypothesis by constructing non-linear stress-strain relationships, rather than on tuning the model coefficients in the turbulent transport equations via ensemble-variational or Kalman filter methods. As recently reviewed [10], a range of machine learning approaches have recently been proposed that can be broadly separated into black box (e.g. Neural Network based) or transparent techniques. Here, a Gene-Expression Programming (GEP) approach [11,12] was used because it yields symbolic expressions that are interpretable. Specifically, the CFD-driven variant [13] of the GEP approach was considered to ensure model consistency of the resulting closures, as can also be achieved with field-inversion [14]. In the CFD-driven GEP method, a RANS solver is integrated with the GEP approach to develop enhanced stress closures. These refined RANS calculations yield more accurate mean flow predictions, which were then utilised in an empirical pressure fluctuation model to achieve better predictions.

2.2. Scope of the experiments, measurement challenges and some relevant modelling observations

2.2.1. Experiment scope

While many more details are given in the source references, it is useful to briefly note the primary quantities analyzed using the data from the experiments of Table 1.

The dimensional documentation of the wind tunnel test section and documentation of conditions in the contraction, at the test section inlet, along the streamwise coordinate in the test section are especially attractive for CFD comparisons, as are the positive and negative range of β investigated. Most of the analysis from the Virginia Tech stereo PIV measurements have to date focused on mean quantities (and the integral quantities these measurements afford) and the turbulent normal and shear stress profiles ($\langle u^2 \rangle$, $\langle v^2 \rangle$, $\langle w^2 \rangle$, and $\langle uv \rangle$) [15], while some analyses of the instantaneous flow features and coherent motions are also on-going [16]. Unique amongst the experiments, those at Virginia Tech also included measurements of surface pressure fluctuations and their statistics and spectra [6,17]. As described further below, this facilitated the GEP turbulence modelling efforts of the Melbourne CFD group.

The primary analyses from the UNH experiments have to date focused on the APG region along the pressure gradient ramp. These include analyses of the mean flow parameters, the $\langle u^2 \rangle$ and $\langle v^2 \rangle$ turbulence normal stresses, the $\langle uv \rangle$ turbulent shear stress, as well as the associated power spectra and cospectra [18,19].

Analyses of the USNA data sets include detailed LDV-based profiles of the mean flow and of various normalisations of $\langle u^2 \rangle$, $\langle v^2 \rangle$ and $\langle uv \rangle$ in the ZPG approach flow, along the FPG-ZPG-APG ramp (see Figure 3). The planar PIV measurements from these experiments have been used to examine average spatial structure (via two-point correlations), and other ensembled features of the turbulence [20,21].

Distinguishing features of the DLR/UniBw experiments are the broad range of β conditions (e.g. up to and beyond separation), the Reynolds number range, and that the measurements were conducted along the ramp, rather than the opposing flat surface. In addition to the aforementioned detailed documentation of the inflow boundary layers, the planar PIV measurements have been to date used to quantify mean flow quantities and turbulent stresses to advance understanding of the mean flow and turbulence fields, as well as quantify upstream history and non-equilibrium flow states [22,23].

2.2.2. Measurement challenges

For the above experiments the well-documented challenges associated with acquiring accurate turbulence measurements (even in the canonical boundary layer flow) persist and in some cases are exacerbated under varying pressure gradient. These challenges include maintaining adequate spatial and temporal measurement resolution (especially at large Re_τ), obtaining reliable and sufficiently dense profile measurements in the near-wall and wake regions, and developing reliable estimates for the friction velocity when the basis for the Clauser plot method becomes questionable. Experiment spatial resolution effects are especially impactful in measurements of $\langle v^2 \rangle$, with particularly large attenuation effects as the wall is approached. In accord with the overall results of the AVT-349 program, the findings herein also reinforce the notion that experiments aiming to further CFD development gain significant value by including specific additional measurements. These include careful documentation of the test section geometry and inflow conditions, error estimates for the measured quantities, and a quantification of non-idealised effects, e.g. deviations from two-dimensionality.

2.2.3. Some observations relevant to modelling

While the specific topics associated with the characterisation of non-equilibrium/flow history effects are addressed in sections 3 and 4 below, it is useful to describe some results associated with the capacity to better model pressure gradient flows, as well as highlight the persistence of distance-from-the-wall scaling – at least under modest pressure gradients.

Gene Expression Programming is also utilised to optimise RANS-enabled estimates of wall-pressure spectra. The previous works [24,25] have demonstrated the effectiveness of a semi-empirical model for wall pressure spectra modelling. Accurate predictions using this model depends, however, on two crucial factors: obtaining precise input data and incorporating the correct relationship between model parameters for prediction.

Traditionally, input parameters from RANS calculations have been employed for noise prediction, due to their efficiency in producing mean-flow predictions. Previous studies [17], however, note that these inputs

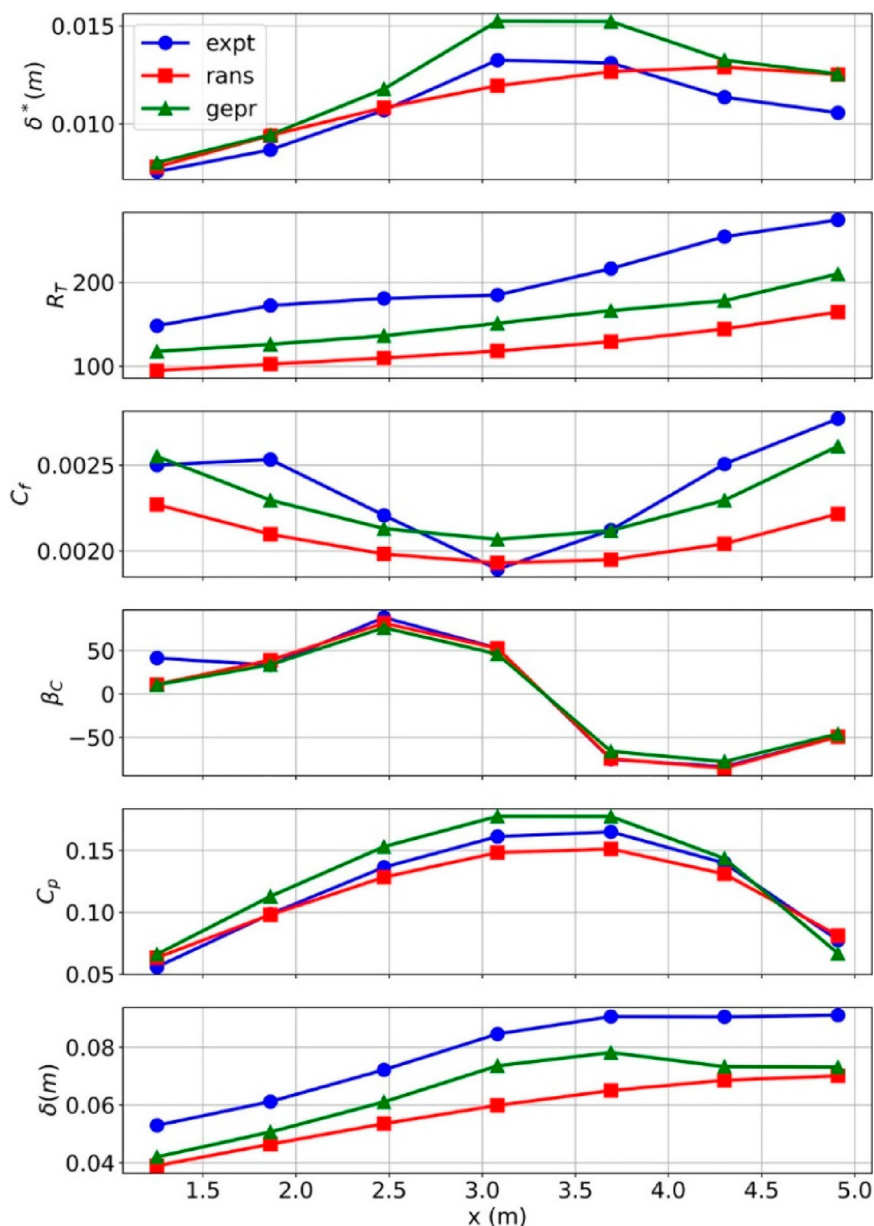


Figure 5. Comparison of experimental boundary layer parameters from baseline RANS and GEP-RANS calculations with values from [17].

can introduce significant errors in the prediction, beyond those attributable to the wall pressure spectrum model itself. To address this issue and improve overall prediction accuracy, the CFD-driven GEP approach was implemented [13] to develop improved RANS closures (denoted as GEP-RANS) providing more reliable mean flow predictions to be fed into the surface pressure spectrum model.

The GEP-RANS approach has been previously explored and validated in a separate study [17], where notable improvements in predicting boundary layer parameters were achieved. Specifically, Figure 5 provides a comparison showing that the GEPRANS results align more closely with experimental data than traditional RANS calculations.

In the study by Shubham et al. [25], a GEP-based surface pressure spectrum model was developed on a combined favourable and adverse pressure gradient training data set and the wall pressure spectrum prediction was shown to outperform existing semi-empirical models. The impact of enhancing the input parameter accuracy through GEP-RANS calculations on the prediction of wall pressure spectra is presented in Figure 6. In addition to using baseline RANS inputs for the wall pressure prediction, the boundary layer inputs to

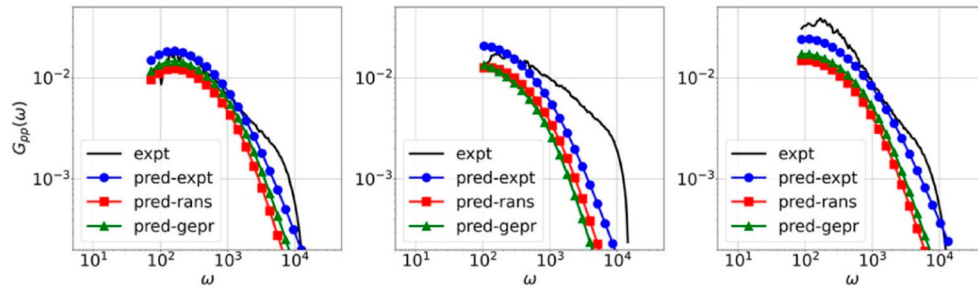


Figure 6. Wall pressure spectrum prediction at $x = 1.86, 3.08, 4.3$ m (left to right) for the $\text{AOA} = 12$ degrees case from the Virginia Tech experiments.

the model obtained from the experiments are also used for comparison. The results demonstrate consistent improvements in peak amplitude predictions for both angles of attack (AOA) considered. Moreover, a noticeable shift towards the predictions with experimental inputs is observed, particularly for $\text{AOA} = 12$ degrees.

From these results it becomes evident that the empirical model is highly sensitive to specific boundary layer parameters. For instance, a more accurate estimation of δ_1 plays a crucial role in enhancing peak amplitude prediction. This analysis emphasises the significance of not only enhancing the empirical wall-pressure model itself but also refining the underlying RANS models for obtaining the essential input parameters.

Distance-from-the-wall scaling plays a central role in many model constructions for the canonical ZPG turbulent boundary layer. Thus, its persistence is relevant when one considers adapting these models to pressure gradient flows. Here it is evidenced that key turbulence statistics continue to scale with the distance from the wall under adverse pressure gradients. The question of wall-scaling has bearing on the continued existence and resilience of the logarithmic mean velocity profile under non-zero pressure gradient, and especially in APG flow, see section 4 below.

The results from the present experiments provide convincing evidence that, to within the accuracy of the measurements, boundary layer turbulence under pressure gradients continues to exhibit distance-from-the-wall scaling. This finding is deemed to be robust for FPG flows, and at a minimum for APG flows up to $\beta \simeq 2$ [18,20]. Regarding the latter of these, Figure 7 shows u and v spectra and uv cospectra from the UNH APG experiments ($\beta = 1.8$) and compares these with ZPG results from the same facility at a similar Re_τ . As is apparent, for both the ZPG and APG flows the spectrograms for v and uv exhibit substantive evidence of wall-scaling within the bounds of the inertial sublayer, as denoted by the vertical lines. This result seems especially compelling for the v spectra – suggesting that, through a scale-selection associated with how they correlate with the u motions, the v motions also underlie the wall-scaling property observed for the inertial layer uv cospectra.

2.3. Executing RANS simulations: key considerations and challenges

As described relative to the entries in Table 2, the RANS simulations incorporated multiple CFD solvers and turbulence models. This section discusses some findings relating to the implementation of the simulations, while Section 5.1 provides an accounting of some of the RANS simulation results and discusses what RANS can and cannot reliably provide relative to the prediction of 2D smooth-wall TBLs subjected to streamwise pressure gradients.

2.3.1. On accurately representing a 3D physical experiment with a 2D computation

A series of CFD experiments were conducted to clarify best practices for representing real test section flows in 2D simulations. For a nominally two-dimensional flow case, as in the 2D bi-directional pressure gradient case from the Virginia Tech experiments, 2D CFD results can provide valuable data and insights at a fraction of the cost of simulating the entire flow. Representing a 3D flow case using 2D simulation requires, however, more than extracting a 2D slice for the computational domain – even for a nominally 2D flow. Wind tunnel test sections can experience a background favourable pressure gradient induced by boundary layer growth

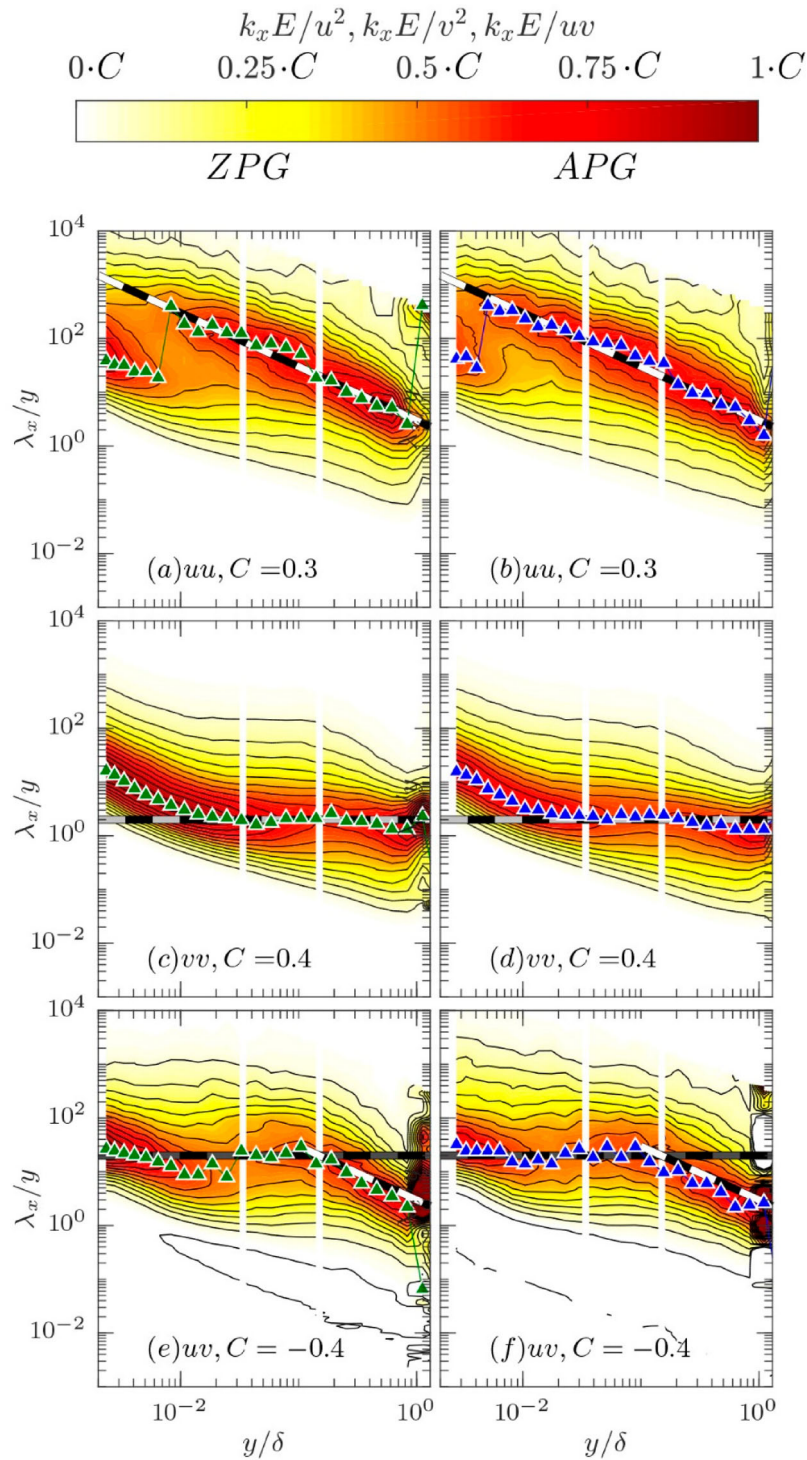


Figure 7. Premultiplied spectra of the streamwise and wall-normal velocity fluctuations and their co-spectra. Left panels are for $\beta = 0$ at $Re_\tau = 7880$ from [47]. Right panels are for $\beta = 1.8$ at $Re_\tau = 7770$. The green and blue triangle symbols represent the peak magnitude of $k_x E$ as a function of wall distance for the ZPG and APG cases, respectively. Vertical white lines denote the bounds of the logarithmic layer. Figure adapted from [18].

on the walls, as well as secondary motions in the test section corners. Similarly, juncture flows will form around any mounted models, model support stings, and instrumentation. A 2D slice of the tunnel does not replicate such complexities. This leads to an incomplete representation of the pressure gradient(s) in the tunnel environment. Here it is also worth noting that simulations intending to reproduce wind tunnel experiments

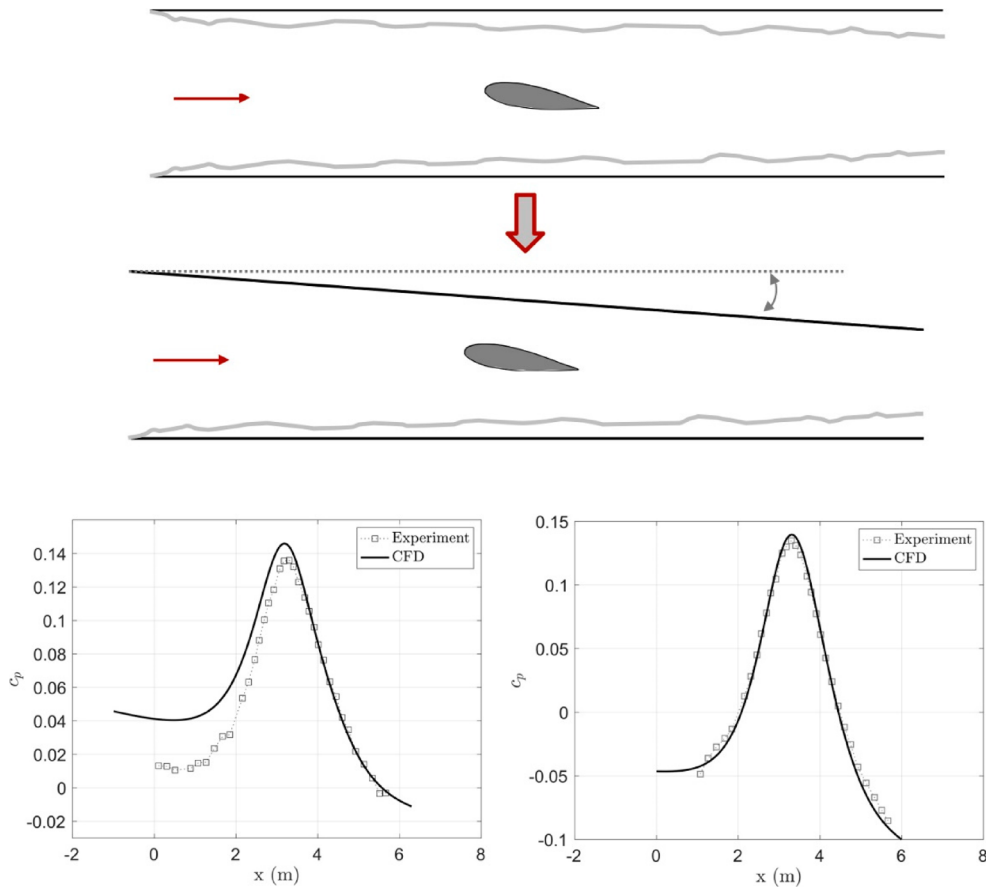


Figure 8. Top: representative diagram illustrating a 2D slice (top) vs. angled top wall (bottom) approach to 2D modelling of airfoil in wind tunnel case. Bottom: pressure distribution simulated with 2D slice (left) and angled top wall (right).

often simulate the model in free-stream flight and thus ignore potential flow effects from the finite extent of the tunnel entirely.

For the bi-directional pressure gradient case, the focus is on how boundary layer growth is affected by the continually varying pressure gradient. Here, the tunnel and mounted airfoil model constitute elements of the boundary value problem that generates overall flow, including the pressure gradient distribution. Thus, these elements are not perturbations to an otherwise existing base flow. During preliminary computations, it was observed that the pressure distribution was effectively impossible to match to experiment due to a bias error, i.e. exactly what would be expected from a mismatch in the background pressure gradient. To address this, a slip flow condition was set for the wall opposite the test wall, and this wall was angled to produce a $P(x)$ that matched with experiment (see Figure 8). While this setup discards the physical wall of the experiment, it apparently yields a superior representation of the operative physics. The general efficacy of this technique is the subject of continuing investigation.

The background pressure gradient in wind tunnel experiments additionally produces other challenges that require careful attention. A primary issue pertains to the definition of the free-stream. The mean streamwise velocity will increase with x in a constant cross-section test section, yet a single value is often reported. Understanding precisely where this value is measured or estimated, and under what conditions and assumptions, is critical to properly replicating the experimental conditions in the simulations. A related extension to this pertains to matching the mean velocity profile inflow condition. As noted previously, in the DLR/UniBw simulations this involved modifying the CFD flow development upstream of the pressure gradient ramp.

2.3.2. Modelling veracity considerations

Discrepancies between the CFD simulations and the target experiment/application can arise owing to a number of issues. As already noted, primary among these is that the experiment is generally only a facsimile of

the actual flow of interest. Thus, implementing a simulation requires targeting either the prediction of the actual experiment, or the actual application. Both of these approaches have merit. The former case allows one to assess the efficacy of the CFD methodology by seeking to replicate the essential non-idealised aspects of the experiment. This, of course, puts additional demands on the documentation and qualification of the experiment(s) (such as accurately measuring the full 3D geometry of the experiment, or quantifying test section corner flows, etc.), and a properly detailed articulation of what is essential in this regard is revisited later. Similarly, if the target is the application, then ‘closing the loop’ between the simulation and experiment requires further assessment of the experiment, but this assessment is relative to properly modelling the application.

Apart from uncertainties associated with the inherent differences between the experiments and simulations, there are also those that stem from the implementation of the simulation itself. The CFD grid constitutes an important source of uncertainty for TBL simulations, and increasingly finer mesh resolution is needed for pressure gradient flows undergoing rapid changes in x . Here, suitable mesh resolution is not only required in the region of interest, but in all regions that substantively influence flow field evolution. For example, Eca et al. [26] demonstrate the need for mesh refinement around the NACA airfoil to properly represent the TBL flow in the Virginia Tech experiment. Inaccuracies are also inherent in the RANS turbulence model, and thus model sensitivity tests are recommended for reliable engineering design applications. Moreover, for the assessment of the predictive accuracy of a RANS model at fullscale-Reynolds-number, the possibility of Reynolds number effects (model scale versus full scale) needs to be kept in mind, as the RANS models are mainly validated for test-cases at model-scale Reynolds numbers [27,28].

3. On characterising nonequilibrium and flow history effects

As referenced at the outset, the notion of nonequilibrium remains difficult to practically capture in a single precise definition. For example, the self-preserving flow definition used by Devenport and Lowe [1] is clear and useful as it captures the symptom that the statistical profiles of such flows are (apparently) immune to invariant representations using locally defined normalising parameters. An ambiguity persists, however, in that an inability to scale profiles could, at least in some circumstances, be a consequence of using the wrong local normalising parameters or combination of parameters. Even so, it is almost assuredly true that many flow situations where self-preserving representations are truly not possible. For example, this may occur when the time scale of some forcing or boundary condition influence is much smaller than the time scale associated with the local flow dynamics, or when dynamical properties reflective of an upstream flow state are rapidly advected into a downstream region. This second scenario seems generically the case where history effects occur in flows with streamwise pressure gradients. Relative to characterising departures from equilibrium, this section first documents the efficacy of the Clauser shape factor across the broad range of β encountered in the USNA experiments. Then the potential for resolvent analysis to capture changes in linear amplification associated with flow history through the mean fields is discussed. The stress budget is then used to describe how more complex velocity scales may be at play, as well as how one might more precisely identify when to expect the onset of a nonequilibrium flow state.

3.1. Clauser shape factor

Equilibrium will occur when the Clauser pressure gradient parameter, β , remains constant. This can be achieved if the freestream velocity varies as $U_\infty = (A(x - x_0))^m$, where A , m , and x_0 are constants. The case with $A < 0$, $x < x_0$, and $m = -1$ is an FPG equilibrium sink flow. An equilibrium APG is produced when $A > 0$, $x > x_0$, and $-0.22 < m < 0$. The limiting cases of $m = -0.22$ and $m = 0$ correspond to a boundary layer at separation and a ZPG flow, respectively. Mellor and Gibson [29] found that for equilibrium boundary layers, the Clauser shape factor, $G = (U_\infty/u_\tau)(H - 1)/H$, is a function of β , as shown in Figure 9 (Note that H is the ratio of the displacement thickness and momentum thickness).

One symptom of non-equilibrium is a departure from the Mellor and Gibson curve. For the points in Figure 9 where $\beta < 0$, an equilibrium ZPG boundary layer was suddenly subjected to a sink flow FPG. This caused an initial shift to the left of the equilibrium curve. Because a sink flow drives the boundary layer toward equilibrium, G decreases and β increases as the flow proceeds in x , approaching the equilibrium curve.

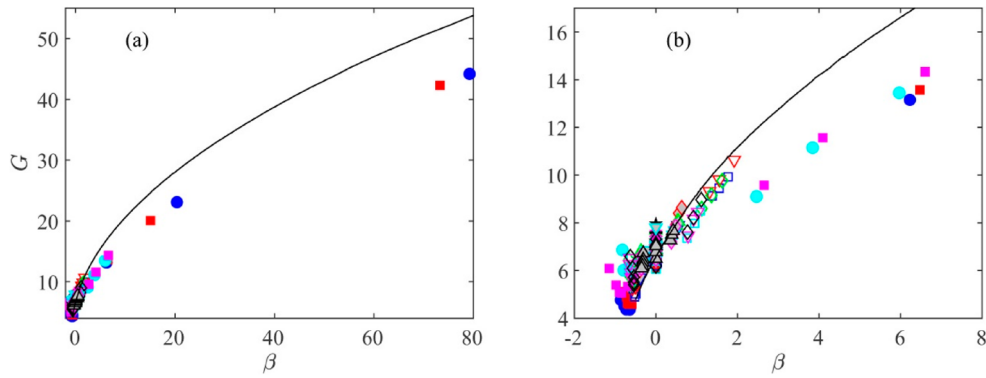


Figure 9. Clauser shape factor versus β compiled from the USNA experiments and literature. The solid line is the equilibrium condition from [29]. Figure adapted from [21].

For the cases with $\beta > 0$ in Figure 9, a ZPG flow is suddenly subject to an APG with a constant, negative acceleration parameter, K . This results in a rapidly growing boundary layer compared to the ZPG case, and a continuously increasing β . An increasing β drives the boundary layer away from equilibrium, causing G to drop below the equilibrium curve in Figure 9. Note that while departure from the equilibrium curve is a sign of non-equilibrium, the converse is not necessarily true. A boundary layer with changing β could conceivably cross the equilibrium curve without having the mean velocity and turbulence profiles in an equilibrium state.

3.2. Linear amplification mechanisms

As discussed above, the history of the pressure gradient impacts the mean field and the turbulent structure of the downstream boundary layer, e.g. [1,30,31]. Resolvent analysis, which takes the mean field as an input to analysis based around the linearised Navier-Stokes operator, offers one means to shed some light into changes in linear amplification associated with different pressure gradient histories encoded in the equations of motion and, explicitly, differences in turbulence structure between ZPG and APG flows.

Resolvent analysis is a tool to analyze the spatio-temporal amplification of the linear Navier-Stokes operator, which is understood to be forced by the terms that are nonlinear in the fluctuations. The biglobal resolvent operator accounts for mean field variations in two directions and thus directly utilises the streamwise variation of the mean velocity and flow history. Knowing the mean fields, basis sets corresponding to the most amplified responses (resolvent modes) to the most dangerous forcing (forcing modes) are obtained by a singular value decomposition of the resolvent, ranked by the singular value or gain. The approach has been extensively reviewed; see, e.g. McKeon [32]. Both operator-driven analysis and a data-driven approach in which the nonlinear weights on the resulting basis functions permits reconstruction of the flow are possible. Here the focus is on what an analysis of the linear resolvent operator reveals about history effects in adverse pressure gradient flows, as explored in Gomez (2023) [33].

We consider boundary layers arriving at nominally identical Re_τ , using the data of Bobke et al. [34] and Pozuelo et al. [35]. The effects of the details of flow history on pressure gradients and mean profiles are shown in Figure 10, along with the changes in the streamwise variance determined from resolvent modes integrated over spanwise wavenumber and temporal frequency and weighted by their singular values for a simplistic rank-1 truncation of the resolvent. The increased amplification in an individual outer layer mode is also shown. For boundary layers arriving at nominally identical Re_τ , upstream histories involving larger values of (weak to mild) adverse pressure gradients lead to a noticeably larger amplification of the larger scales in the outer part of the flow. Of course, the wake field is extended in APG flows, resulting in a larger wall-normal extent (and a larger range of convection velocities) for resolvent mode development. On the other hand, inner scaling continues to hold where the mean profile remains (nominally) self-similar with the ZPG case – both consistent with the properties of the resolvent operator and experimental observations. As evidenced, resolvent analysis, with and without nonlinear basis weights, holds promise as an efficient means of gaining insight into structural changes associated with history effects in APG flows.

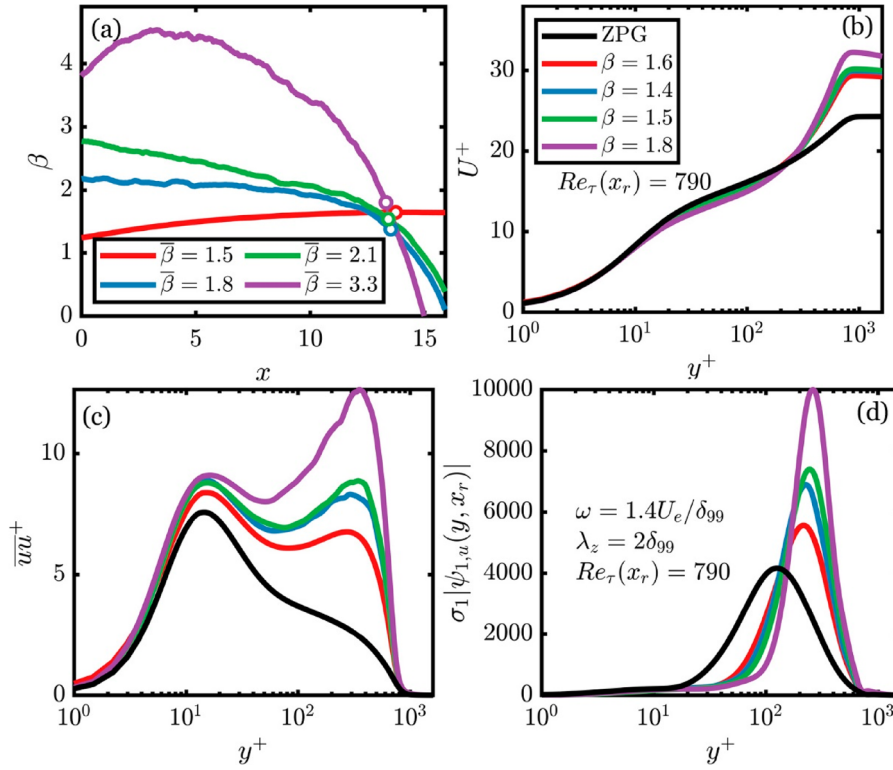


Figure 10. Biglobal resolvent analysis captures changes in linear amplification associated with pressure gradient history [33]. (a) Pressure gradient histories considered, from [34,35]. Open circle denotes the Reynolds number for comparison of model results, $Re_\tau = 790$. (b) Associated mean streamwise velocity profiles at $Re_\tau = 790$. (c) Variation of streamwise fluctuation variance. (d) Amplification (sigma)-weighted shape of the streamwise component of the first resolvent mode at the comparison point in (a) captures the increased outer layer energy associated with larger average β values.

3.3. Stress budget for pressure gradient flows

As discussed further in Section 4 below, for flow far from separation the mean dynamical equation for the 2D flows considered herein contains a non-zero pressure gradient force. Accordingly, the once integrated form of this equation has an effective pressure stress-related term that is absent in the stress budget for the ZPG flow.

$$v \frac{\partial U}{\partial y} + \langle -uv \rangle + \int_0^y \left[-U \frac{\partial U}{\partial x} - V \frac{\partial U}{\partial y} \right] dy = u_\tau^2 + \left(\frac{y}{\rho} \frac{dP}{dx} \right) \quad (1)$$

In order, the terms on the left of equation 1 comprise the viscous shear stress, Reynolds shear stress and the mean inertia integral (mean inertial stress). These are the same terms that appear in the stress budget for the ZPG boundary layer. The right side of this equation, however, contains the additional stress-like quantity that is the product of y and the pressure gradient that varies in x . At the wall, the non-zero terms in this equation are u_τ^2 and the mean viscous stress, while in the freestream, they are the mean inertial stress, the pressure stress and u_τ^2 .

Romero et al. [30,36] consider the implications of equation (1), two of which are now described. The first is that its construction suggests that a hybrid velocity scale,

$$u_{hyb}^2 = u_\tau^2 + \left(\frac{y}{\rho} \frac{dP}{dx} \right) \quad (2)$$

is relevant to pressure gradient boundary layers. In this regard, Romero et al. demonstrated that u_{hyb} does indeed generate (nearly) invariant profiles of the turbulent stress profiles for sufficiently moderate variations in β under adverse pressure gradient conditions. Note that the u_τ contribution to u_{hyb} is naturally dominant near the wall, while the pressure stress contribution increases with y . The second implication of equation (1) is associated to the conditions under which u_{hyb} scaling apparently breaks down. Here, Romero et al.

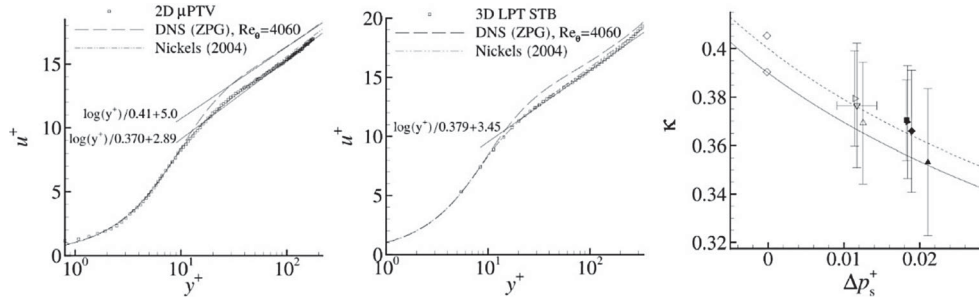


Figure 11. Mean-velocity profile and least-squares fit in the log-law region at $\Delta P_s^+ = 0.0183$ (first panel), and for $\Delta P_s^+ = 0.0114$ (second panel). Last panel shows the measured reduction in the von Karman constant for increasing ΔP_s^+ . Figures adapted from [22].

[36] considered the stress budget for rapid variations in β from the data set of Bobke et al. [34]. This analysis revealed that the breakdown of u_{hyb} scaling corresponds to the condition in which the balance of the dominant terms in the stress budget changes. This led Romero et al. to conjecture that this attribute may in fact be a generic indicator of when the flow has entered a non-equilibrium state.

4. On the resilience of the logarithmic mean velocity profile under pressure gradient

Measurements from the present experiments, in concert with existing previous measurements, are considered to first provide a summary of empirical evidence regarding the persistence of the logarithmic mean velocity profile in pressure gradient flows. This is then followed by semi-theoretical analyses exploring why a logarithmic profile might or might not persist.

4.1. Experimental observations

Knopp et al. [22,37] generated a summary of experimental observations of log layer data, and interpreted these relative to measurement uncertainties. This study considered data from APG TBLs from wind-tunnel experiments, DNS and LES. For mild to moderate APG, these analyses found that, to within the data uncertainty, there exists region where the mean data follow a profile adhering to

$$U^+(y^+) = \frac{1}{\kappa} \ln(y^+) + B \quad (3)$$

Characteristics of this region of logarithmic profile, however, display variations with pressure gradient that Knopp et al. [22] quantified in Figure 11. Here they used the inner-normalised pressure gradient along the surface, $\Delta P_s^+ = \nu/(\rho u_\tau^3) dp/ds$. In this regard, note that for the profile of Figure 11(a) $\Delta P_s^+ = 0.0183$ is equivalent to $\beta = 26.37$. Overall, the analyses of Knopp et al. [22] show that for increasing APG the values of κ and B in equation 3 decrease. Additionally, the results of [37] reveal that the outer-normalised extent over which equation (3) holds also decreases with increasing ΔP_s .

The aim of the DLR/UniBw experiment was to assess a theoretical model for κ by Nickels [38]. The model assumes that the mean-velocity-gradient scaling in the inner layer in pressure gradient is given by $\partial U/\partial y = U_T/(\kappa_0 y)$. Here, κ_0 is the value of κ in a TBL at ZPG and U_T is a velocity scale associated with the total shear stress at the outer edge of the viscous sublayer y_c . Note that the thickness of the viscous sublayer y_c is assumed to depend on ΔP^+ (which is another part of the model by Nickels for the inner layer). If the actual κ is defined via the traditional formulation $\partial U/\partial y = u_\tau/(\kappa y)$, then comparing the two relations for $\partial U/\partial y$ suggests that $\kappa/\kappa_0 = u_\tau/U_T = 1/\sqrt{\{(1 + P_s^+ y_c^+)\}}$. The curve $\kappa(\Delta P_s^+)$ is plotted for two values of κ_0 in Figure 11(c).

The measurements and analyses of Volino [20] provide a lower Reynolds number complement to those of Knopp et al. [22,37] that includes consideration of FPG flows. As shown in Figure 12 below, the APG results generally agree with the conclusions of Knopp et al. [22], while the FPG results suggest an increasing region of apparent logarithmic profile, although for sufficiently large FPG the existence of a purely logarithmic variation

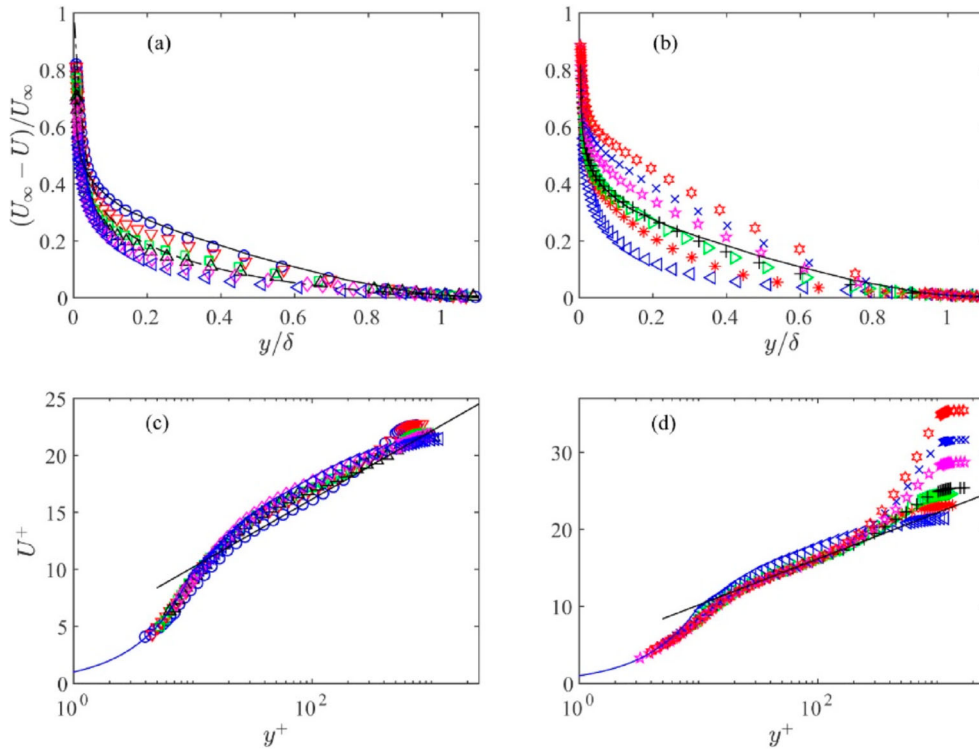


Figure 12. Mean streamwise velocity profiles from the case 2 ramp of the USNA experiments. Favourable pressure gradient flows are plotted in the first column. Adverse pressure gradient flows are plotted in the second column. The top figures are outer-normalised and the bottom figures are inner-normalised. Solid lines denote that canonical ZPG flow with $\kappa = 0.384$ and $B = 4.2$, dash-dot lines denote sink-flow DNS [41]. Figures adapted from [20].

becomes questionable, as the profile begins to exhibit apparent curvature when plotted on semi-logarithmic axes.

4.2. Semi-theoretical considerations

This section provides some analysis based perspectives that have bearing on the persistence of the logarithmic mean velocity profile under pressure gradient. The first uses a mixing length construction from which to pose questions relative to the empirical observations. The second bases its discussion on the observed changes to the terms in the RANS equations.

4.2.1. Logarithmic behaviour: what mixing length arguments suggest

There are several methods for arriving at the logarithmic mean velocity profile observed in ZPG boundary layers. One that may be instructive for considering the nonequilibrium cases is the argument that the log-law in a ZPG follows from the Prandtl mixing length assumption for turbulent momentum transport. Taking the streamwise momentum equation for a steady, two-dimensional boundary layer and applying the Couette flow assumption (the streamwise gradient of velocity term is small in the inner part of the boundary layer and may be neglected), one obtains in inner coordinates

$$\frac{\tau}{\tau_w} = 1 + P^+ y^+, \quad (4)$$

where $\tau = \mu dU/dy + \rho \langle uv \rangle$ is the local shear stress, τ_w is the wall shear stress, and

$$P^+ = \frac{\mu dP/dx}{\rho^{1/2} \tau_w^{3/2}} = \frac{\beta U_\infty^+}{Re_{\delta_1}}. \quad (5)$$

Here, Re_{δ_1} is the Reynolds number based upon U_∞ and δ_1 (displacement thickness), both of which are functions of x .

For purposes of illustration, we now assume that outside the viscous sublayer and buffer region the effect of viscosity is small relative to turbulent mixing, and that $\tau / \rho = \nu_T dU / dy$, where $\nu_T = \ell^2 dU / dy$ is the eddy viscosity and ℓ is the mixing length. Now, if the mixing length varies linearly with distance from the wall, $\ell = \kappa y$, equation (4) becomes

$$\frac{dU^+}{dy^+} = \frac{(1 + P^+ y^+)^{1/2}}{\kappa y^+}. \quad (6)$$

For the ZPG case, $P^+ = 0$ and integration of equation (6) results in the canonical logarithmic profile with slope κ^{-1} . In this formulation, the logarithmic law and the mixing length assumption imply and require each other. For the non-ZPG case, equation 6 clearly does not result in a logarithmic profile, also see Townsend [39]. This, however, does not preclude the existence of a logarithmically varying U in non-ZPG cases since the assumption that $\ell = \kappa y$ may no longer hold. Logarithmic dependence could, however, be recovered if $\ell = (1 + P^+ y^+)^{1/2} \kappa y$. This relation for the mixing length does not appear to be impossible in all cases, but it does seem unlikely as it would, for example, result in imaginary values of ℓ for some FPG cases. Hence, arguments along these lines suggest that the velocity profile is probably not exactly logarithmic in pressure gradient boundary layers.

In the absence of perfect logarithmic dependence a pertinent question is how significant is the deviation? For equilibrium sink flow FPG cases there is evidence in experiments such as those of Jones and Launder [40], the DNS computations of Spalart [41], the more recent DNS of Yuan and Piomelli [42], as well as the USNA experiment results in Figure 12. For the highest values of K (the inner normalised pressure gradient) the mean profile shifts upward in U^+ from the canonical ZPG profile by about 4, while the shape and slope of the profiles do not vary greatly from the ZPG case. Further increases in K initiate relaminarisation. For APG cases the results are less clear. As shown in Figure 12d, an APG causes growth of the wake, which encroaches on the log-linear region and reduces its extent in terms of y^+ . For the moderate Reynolds number cases of 12d, the shift in U^+ from the ZPG log-law is at most modest for the pressure gradient shown. The slope does not appear to change, but with the log region extent reducing to less than a decade in y^+ it is difficult to draw any firm conclusions. Increasing Re_τ will likely increase the extent of the log region. This, however, would result in a smaller P^+ at fixed β . Equation (6) suggests that as P^+ decreases the deviation from logarithmic behaviour should also decrease. If β and Re_τ were simultaneously increased, it is rationally expected that the wake would again become large and decrease the extent of the log region, as in Figure 6. The existing APG results suggest that the log region will tend to disappear before a large deviation from the ZPG log-law becomes observable. If this is indeed true, it is an encouraging result for those using the modified Clauser method (fitting the mean flow velocity profile to the canonical log-law) to determine u_τ from APG experimental data.

4.2.2. Ramifications of changing the mean force structure

The mean momentum equation for the 2D ZPG boundary layer is given by

$$\rho \left(U \frac{\partial U}{\partial x} + V \frac{\partial U}{\partial y} \right) + \rho \frac{\partial \langle uv \rangle}{\partial y} = \mu \frac{\partial^2 U}{\partial y^2} \quad (7)$$

This equation has the dimensions of force or inertia per unit volume. The terms on the left comprise the mean inertia (MI) and mean effect of turbulent inertia (TI), while the term on the right is the mean viscous force (VF). For pressure gradient flows not too close to separation, the mean equation becomes

$$\rho \left(U \frac{\partial U}{\partial x} + V \frac{\partial U}{\partial y} \right) + \rho \frac{\partial uv}{\partial y} = -\frac{dP}{dx} + \mu \frac{\partial^2 U}{\partial y^2} \quad (8)$$

The structural changes concomitant with the addition of the pressure force in equation (8) indicate a significantly more complicated force balance in the inertial domain where logarithmic dependence is expected, as well as provide reasons (now given) to suspect that exact logarithmic behaviour is highly unlikely in pressure gradient flows.

The changes just noted are made apparent in the profiles of terms in Figure 13. In the ZPG case there are only three terms and thus from Figure 13(a) it is clear that near the wall the dominant balance is between the TI and VF terms while beyond the zero-crossing of the TI term (peak in $\langle uv \rangle$) the dominant balance is

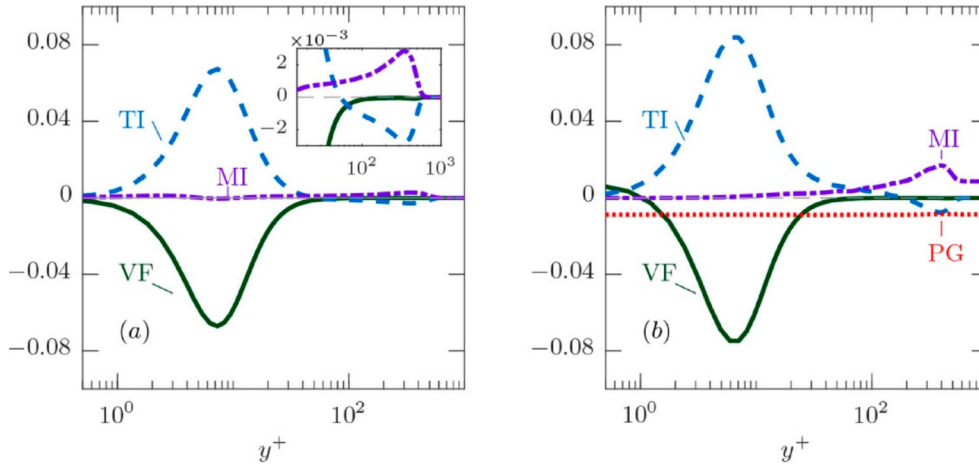


Figure 13. Terms in the mean momentum balance for: ZPG flow at $Re_\tau = 490$ from [48] (left), APG flow at $Re_\tau = 490$ for $\beta \simeq 1.2$ from [34]. Figure adapted from [18].

between the TI and MI terms. It is on the interior portion of inertial domain where logarithmic dependence is observed and analytically predicted, e.g. see Romero et al. [18] and the references therein. The case of an APG flow at the same Re_τ and modest β is shown in Figure 13(b). Key observations here are that the VF term continues to lose leading order at about the same y^+ location for fixed Re_τ , while the zero-crossing of the TI term has moved dramatically outward. As is apparent, the inertial balance beyond where the VF term becomes negligible now involves three terms and is qualitatively distinct from the ZPG flow in that the TI term is now positive on the logarithmic layer.

Regarding behaviour of the TI term, close scrutiny of APG flows reveals that the outward shift in its zero-crossing from positive (momentum source) to negative (momentum sink) occurs rapidly and between $0 < \beta < 1$. This has consequences on how the mean equation admits a solution [18]. Furthermore, this outward shift is consistent with the analysis of Wei and Knopp [43] that yields an outer scaling for APG flows, and also suggests that this outer scaling probably holds to where the VF term loses leading order (i.e. much closer to the wall). As noted in the previous section, integration of equation (8) reveals that the stress budget has non-zero values at the inner and outer boundaries. This supports the conclusion that the APG flow has two contributing velocity scales [19]. Analysis of the mean equation using the methodology of Fife et al. [44] indicates that a two velocity scale situation will generically lead to a power law rather than a logarithmic profile solution [18]. Thus, while the empirical observations suggest a persistence of the logarithmic layer (at least to within the uncertainty of the data), analyses such as just described suggest that the purely logarithmic flow (say, as associated with the ZPG flow as $Re_\tau \rightarrow \infty$) is unlikely under pressure gradient conditions.

5. On computing pressure gradient TBLs using RANS simulations

The following sections first present a number of comparisons between different simulations (CFD solvers and turbulence models) and the experiments. This is followed by a summary and discussion regarding the capabilities and limitations of RANS relative to predicting 2D smooth-wall TBLs subjected to pressure gradients, as well as some commentary regarding open questions relevant to advancing the predictive capability of RANS.

5.1. Findings from RANS simulations

Figure 14 presents RANS simulation results for 2D, low Mach number, large Re_τ smooth wall boundary layers subject to the bi-directional pressure gradients of the Virginia Tech experiments. Results from multiple solvers exhibit substantive agreement in both solver-to-solver and solver-to-experiment comparisons. Overall, these results evidence that RANS can produce accurate results for both FPG and APG conditions – at least for the range of β considered.

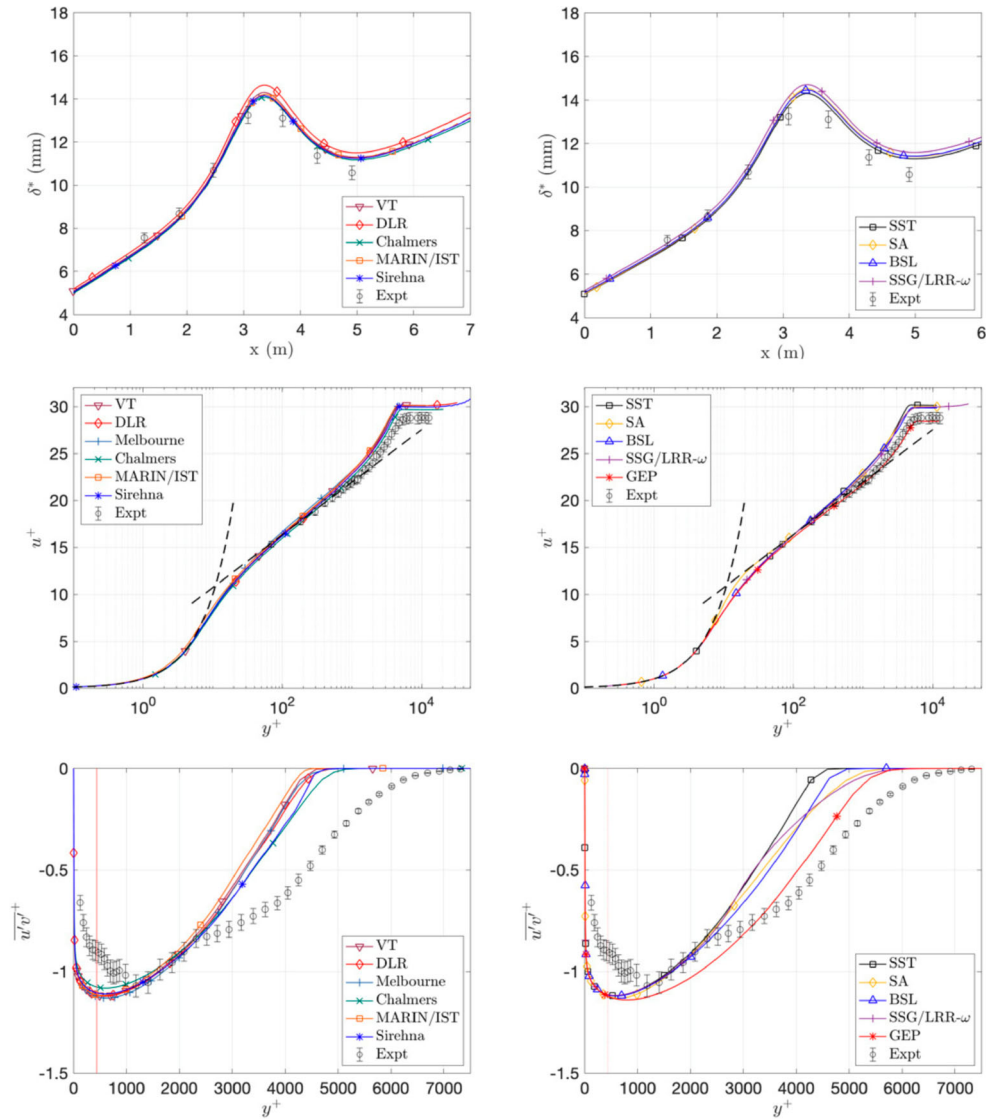


Figure 14. Selected results for 2D simulations of bi-directional adverse-to-favourable pressure gradient case at $Re_c = 2 \times 10^6$. Left-column: results produced using varying RANS solvers. Right-column: results produced using varying turbulence models. Top row: displacement thickness as a function of wall position. Middle row: inner-normalised mean velocity profiles at the position of dp/dx_{\max} in top row. Bottom row: inner-normalised uv profiles at the position of dp/dx_{\max} in top row. Figures adapted from [17].

The results of Figure 14 further indicate and that the different RANS solvers produce identical or nearly identical results. This finding, however, comes with the following caveats: (i) the RANS solutions are obtained on the same grids, (ii) the grids have been chosen based on a suitable grid refinement study, (iii) solution residuals are converged to at least six orders of magnitude, and (iv) the exact same turbulence model and model coefficients are used between comparable simulations. While seemingly restrictive, this conclusion still implies that variations in solver algorithms, flux schemes, and limiter schemes do not have statistically significant effects on the present RANS solutions.

Variations in RANS solutions do, however, arise between different turbulence models and between compressible and incompressible solution schemes. At a Mach number of approximately 0.1, this case lies in the overlap range where both compressible and incompressible solvers could be considered stable and valid. They produce, however, small solution differences, and particularly in the pressure distribution. A variation with turbulence model might be expected, but is encouragingly small in this case.

The same agreement can be achieved with a 3D simulation provided that the pressure gradient distribution is accurately captured (see Figure 15). This is of substantive importance and presents challenges for modelling.

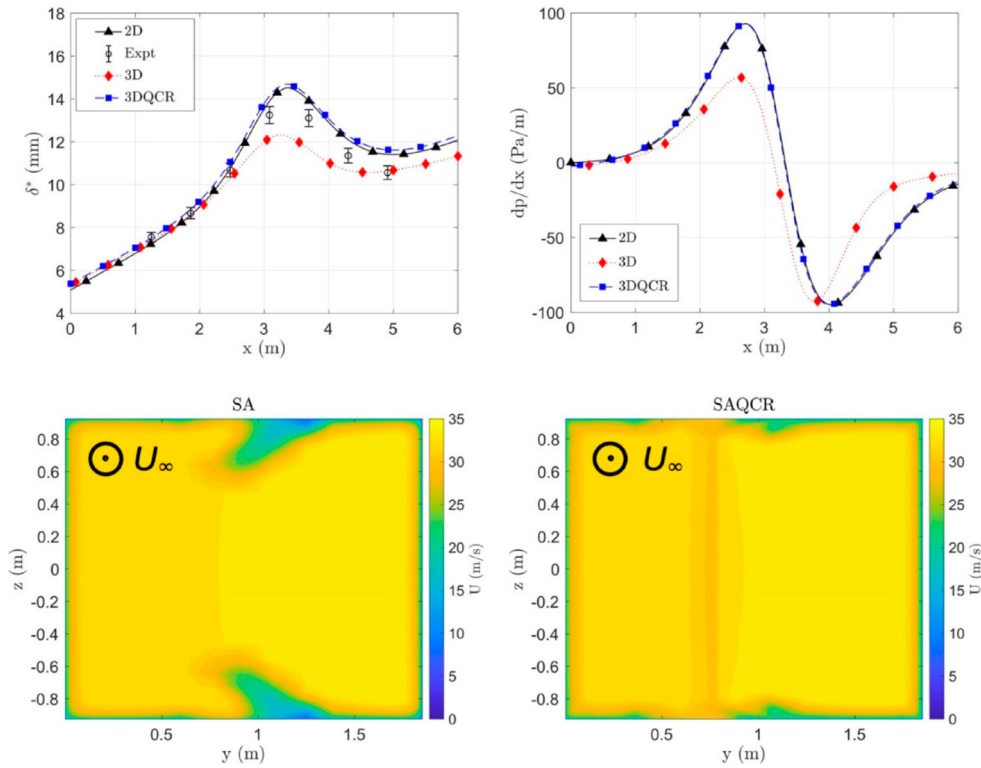


Figure 15. Selected results for 3D simulations of bi-directional adverse-to-favourable pressure gradient case at $Re_c = 2 \times 10^6$. Top-left: displacement thickness produced by various turbulence models. Top-right: pressure gradient distribution predicted by various turbulence models. Bottom-left: streamwise velocity contours in the cross-sectional plane using standard Spalart-Allmaras model. Bottom-right: streamwise velocity contour in the cross-sectional plane using SAQCR model.

In the 2D simulations, the wall pressure gradient is a function of the forces on the 2D NACA0012 airfoil and the background favourable pressure gradient produced by the angled wall, both of which are re-produced well in a RANS environment. Conversely, in the 3D simulation the pressure gradient is additionally a function of the corner and junction flows where the airfoil model meets the bounding walls. Generally speaking, RANS models do a poor job of simulating secondary flow phenomena, resulting in a modelled $dP/dx(x)$ profile that does not match experiment. This point is demonstrated in Figure 16. The addition of a Quadratic Constitutive Relation (QCR) turbulence model changes the junction and wake flows behind and around the airfoil model considerably and produces a dP/dx distribution and boundary layer growth profile that matches experiment and the 2D simulation data. Here we note that the angled-wall 2D case was assessed with both SSTQCR and SAQCR and it was observed that there was no difference between the QCR and linear versions of the respective models for the 2D case. Non-linear constitutive relations have been shown to be necessary for reproducing secondary flow phenomena, particularly secondary flows of the second kind. As a comment, the quadratic constitutive relation (QCR) is an example of a non-linear constitutive relation in the larger class of algebraic stress models (ASM) and explicit ASMs (EASM). The quadratic constitutive relation (QCR) is one example of the larger class of non-linear constitutive relations, including algebraic stress models (ASM) and explicit ASMs (EASM), but only QCR models were investigated here.

Consider further the situation for strong APGs ($\beta \geq 20$) and the findings for the DLR/UniBw flow. The experiment was designed to obtain an attached boundary layer flow subjected to a strong APG (β around 26). Regarding this case, Knopp et al. [37] showed that RANS simulations using the SSG/LRR- ω model over-predict the mean velocity in the inertial sublayer. While this over-prediction is likely to be influenced by the mild convex curvature in the non-equilibrium region upstream of the APG region (indicated by predictions using SA with a modification to account for curvature effects, SA-RC compared to SA), there are reasonable indications that the first-order effects are attributable to the APG. This conjecture is supported by similar observations of mean velocity over-prediction, for the equilibrium TBL on a flat plate, in a strong APG flow ($\beta_{RC} = 20$) [45], and as found for different RANS models [46]. In this study, 3D simulations of the test-case

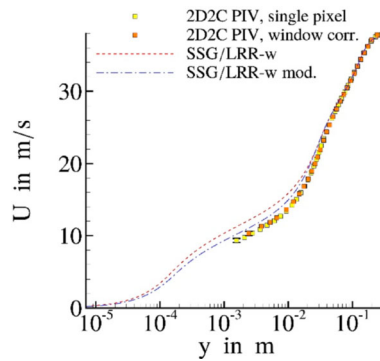


Figure 16. Mean velocity profile for the DLR/UniBw turbulent boundary layer flow in the strong APG region.

by Skare and Krogstad [45] using different Reynolds stress models and SA-RC-QCR were made to account for the corner vortices, which is required to accurately describe the C_p -distribution along the wind-tunnel centerline (see figure 4.11 of [46]). The second common observation was the under-prediction of $\partial U^+/\partial y^+$ in the inertial sublayer – a result found in both the simulations of the DLR/UniBw flow and the flow studied by Skare and Krogstad.

Figure 16 illustrates these observations. Here the mean velocity is given for $x = 10.09$ m in the strong APG region ($\Delta p^+ = 0.018$). As can be seen, the SSG/LRR- ω model over-predicts the mean velocity in the inertial sublayer. The figure includes the results for the SSG/LRR- ω model with APG modification, see Knopp et al. [37]. Conversely, the modified model reduces the mean velocity in the inertial sublayer, leading to improved agreement with the experimental data.

5.2. On the predictive capabilities of RANS

We now provide some discussion, commentary and perspectives (and counter perspectives) on (i) what RANS can compute relative to 2D smooth-wall boundary layers subjected to pressure gradients, and (ii) what are the rational next steps regarding the advancement of RANS as a predictive tool.

The following observations are noted under the provision that the RANS simulations were conducted with proper attention to the error and uncertainty considerations noted in section 2.3 and also use a sufficiently fine grid with appropriately placed refinement zones and sufficient convergence. These requirements lead to sufficiently small numerical uncertainties. A substantive variety of the RANS based computations exhibited encouraging levels of success relative to predicting boundary layer growth in tripped/fully turbulent boundary layers. Similarly, almost all of the RANS simulations of near-equilibrium flows (generally characterised by mild pressure gradients) were able to produce mean velocity profiles that comported with experiments – at least to within the experimental uncertainty. Additionally, RANS does generally seem to hold promise relative to capturing local pressure gradient effects on mean flow behaviour. This, however, depends somewhat on the severity of the local effect. Similarly, RANS simulations showed some levels of success in capturing history effects, albeit this comes with some relatively significant provisos pertaining to the simulation's ability to capture the evolution of the mean flow and pressure gradient. This rather clearly seems to be an area requiring continued investigation. Similarly, while the capacity of RANS simulations to correctly predict more comprehensive quantities, such as mean forces and moments, remains substantively dependent on meshing and model choices, etc., RANS simulations can generally be trusted to produce reliable predictions.

Relative to the present 2D flows, there are complexities that RANS cannot handle that arise relative to comparisons with physical experiments. These largely pertain to the inability of the physical experiments to accurately represent the idealised conditions, such as 2D flow, that can be exactly prescribed in a simulation. These effects are, for example, manifest by the formation of corner secondary flows that, relative to pressure gradient and history effects complicate the flow development prediction because the inherent 2D assumption is violated. As discussed further in the Conclusions, the perspectives of the AVT-349 team are somewhat mixed on what is the best future research response to this issue. As highlighted in the previous section, RANS simulations require further refinement relative to strong pressure gradient effects, while the

accurate prediction of the turbulent stresses, and their evolution under pressure gradients, remains an active area of investigation. Lastly, an issue that is critically important to many technologies pertains to the capacity of current RANS formulations to capture Reynolds number dependence. As evidenced by the MARIN team's comparisons at ship-scale Reynolds numbers, even key mean flow parameters, such as κ , exhibit variations from low Reynolds number results when application scale Reynolds numbers are considered.

6. Conclusions

In this section we first describe the primary results and conclusions from the experimental observations. This is followed by a summary of findings relative to both the implementation and capabilities of RANS for the flows under consideration. The section concludes with a discussion of open issues and the identification of priority areas requiring further investigation.

6.1. Primary new findings and perspectives

Conclusions drawn here derive in part from the experiments described in Table 1 as well as from previous studies. Observations regarding the mean velocity profile indicate that, to within the accuracy of the measurements, a logarithmic layer nominally persists under pressure gradient conditions. For sufficiently large favourable pressure gradients, the data begin to exhibit apparent deviations from a linear profile when plotted on semi-log axes, while the application of sufficiently large adverse pressure gradients show an encroachment of non-logarithmic influences from the outer region. This is manifest in the upper bound of the log layer diminishing when measured relative to δ . A finding connected to this is that, like in the canonical ZPG flow, the pre-multiplied v spectra and uv co-spectra in APG flows up to modest β exhibit clear evidence of distance-from-the-wall scaling across an interior domain. This behaviour, however, does not necessarily point to the existence of a logarithmic mean velocity profile, as the present experiments also suggest that the u_{hyb} velocity scale for pressure gradient flows incorporates contributions from both the wall shear stress and a pressure stress term that varies with y – see equation (2).

As described at the outset, for pragmatic reasons the present study adopted the condition of self-preserving flow as a point of distinction regarding the definition of equilibrium versus non-equilibrium flow. The best way to define these terms, however, remains a matter of debate. The mean flow based discriminator of flow state adopted, which is reflected in measures such as the Clauser shape factor (see Figure 9), requires an a priori specification of the characteristic length and velocity scales. Thus, if one were to use incorrect characteristic scales an incorrect interpretation of non-equilibrium flow might result. Other measures of non-equilibrium, such as an imbalance between turbulence kinetic energy production and dissipation, look to the properties of the turbulence kinetic energy budget to define, or at least characterise, distinguishing traits. Similarly, an analysis described herein suggests that the breakdown of u_{hyb} scaling stems from a qualitative change in the leading order terms in the mean stress budget. Whether this criterion is a general way of delineating an equilibrium versus non-equilibrium condition, however, requires further investigation.

Whatever the deviation from non-equilibrium under this definition, the resolvent provides a modelling method capable of capturing trends in structural changes to the turbulence as encoded through the spatial variation of the mean velocity field, and thus the details of the pressure history. Just as the Gene Expression Programming described herein gives insights into prediction of the wall pressure fluctuation spectrum, resolvent analysis gives insight into the most amplified disturbances for a given mean field, and explicitly the differences between ZPG and APG flows. As such, the approach has the potential to provide a natural link between the mean fields from experiment, or predicted by RANS, and the turbulence itself. Of note is the ability for the analysis to identify the effects of different pressure gradient histories.

Conclusions pertaining to RANS simulations primarily stem from the efforts summarised in Table 2. Overall, the present findings indicate that for other variables held fixed, different RANS solvers produce the same results for boundary layers subjected to pressure gradients. In this case, observed variations are therefore likely to arise owing to the properties of the grid, turbulence model, or convergence criteria, as opposed to the solver itself. As it pertains to reproducing experimental observations, a major issue is that the velocity field in a wind tunnel typically contains complex corner and junction flows. Generally speaking, RANS simulations do not accurately capture such complexities, and this presents significant challenges to model development

and validation for the primary flow phenomena of interest. For example, modelling the tunnel experiment with a *clean* 2D free-stream flow excludes key flow physics inherent to the experiment, while modelling the actual flow in the tunnel is likely to produce erroneous results owing to the inability of the RANS simulation to capture the 3D flow features in the physical flow. Overall, it is concluded that CFD development is advanced by experiments that include specifications of the test section geometry, documentation of the inflow conditions, comprehensive error estimates for the measured quantities, and an accounting of deviations from two-dimensionality.

Beyond the comparison issues just noted, a broader conclusion is that RANS simulations performed well and exceeded expectations relative to capturing pressure gradient and downstream history effects – at least under modest pressure gradient conditions. Additionally, with regard to RANS-based wall pressure fluctuation prediction, the GEP approach has the apparent benefits of improving empirical closure models while also determining the essential input parameters needed to predict wall pressure statistics.

6.2. Substantive open questions

As it pertains to the future of RANS simulations, the AVT-349 team seemed to hold three perspectives: (i) RANS in its present state of development is sufficient, (ii) RANS in its present state is unsuitable to meet current needs, and thus further investment in its improvement is warranted, and (iii) RANS is fundamentally limited and unsuitable and thus other more advanced CFD methods are needed. Currently, it would appear that item (ii) constitutes a relatively small minority of users, and there are many varied opinions on what should be prioritised within that group, e.g. weighing the relative strengths and weaknesses of eddy-viscosity models, QCR modelling, Reynolds-Stress-Transport modelling and improved validation methodologies. With regard to these, we also make note of specific open questions that, in part, prompt opportunities for future work,

- What are the parameters suitable to characterise the strength of departure of a turbulent boundary layer from equilibrium?
- What are the primary effects of a large departure from equilibrium on the mean flow and turbulence statistics, and what are the implications of such flow situations for the overall performance of aero/naval vehicles?
- Why do QCR models seem to work well for juncture/corner flows and how do they compare to other non-linear constitutive relation models and to full differential Reynolds-Stress-Transport models?
- What methodology is best for validating CFD with physical experiment data, and what are the most important elements of the wind tunnel experiment and simulation that need to be most closely matched?
- What is the limiting pressure gradient (approximately) at which RANS simulations fail to provide reliable results, and what is the physical reason for this limit?
- What is known for flows involving a combination of pressure gradient and surface curvature effects? (A lack of systematic experimental studies is in contrast to the high relevance for many technologies involving flow separation on smoothly curved bodies.)
- What are the first order history effects that need to be better modelled, and what history effects (such as in 3D flow) are beyond the scope of RANS modelling?

6.3. Priorities for future research

The above, necessarily incomplete, list of open questions naturally prompts the need for future research. Broadly speaking, a deeper understanding of the qualitative effects of non-equilibrium on the dynamical behaviour of the boundary layer dynamics is needed. In concert with this, a database covering a systematic variation of pressure gradients and the streamwise distance over which the pressure gradient is applied would allow proper parameterisation of both the mean flow and Reynolds stresses. From the viewpoint of a design engineer, empirical quantitative criteria as to whether certain non-equilibrium conditions make a boundary layer more prone to flow separation (or, conversely, might reduce the susceptibility for separation) would also be useful. Here, data from DNS/LES would provide information on the full Reynolds stress budget and thus foster a deeper understanding of non-equilibrium in terms of the Reynolds stress balance – albeit at

low Reynolds numbers. It is thus also noteworthy that DNS/LES data could aid in assessing wind-tunnel data for 2D flows, as evidenced by the test-cases highlighted herein.

The physics (or lack thereof) of QCR models requires clarification. As for CFD validation, there seems to be incomplete agreement pertaining to whether it is better to put more effort toward tailoring the simulation to match the details of the wind tunnel experiments, or to work more diligently to make the physical experiments coincide with the idealisations of the simulation. Here, the focus of the given effort would colour which choice is most appropriate. Under either case, however, systematic and well-documented studies that clarify which aspects of the experiments are the most important to match in the simulation seem well-justified. With regard to theory, there remains much yet to uncover regarding the mathematical characterisation of pressure gradient history effects. More broadly, this includes determining a more mathematically (and physically) precise specification of what constitutes a non-equilibrium condition along with a specification of the measurable symptoms associated with the transition from an equilibrium to non-equilibrium state.

Lastly, an additional relevant flow phenomenon in many technologies that occurs in conjunction with pressure gradients and non-equilibrium effects is surface curvature. In the past, curvature effects and pressure gradient effects were mostly studied separately, or the test-cases used a fixed combination of pressure gradient and surface curvature, e.g. as in the DLR/UniBw experiments. Further systematic investigations covering a broad range of conditions in which both curvature and pressure gradient effects are subject to parametrised variations would thus fill an important need. The lack of experimental studies seems to be in contrast to the high relevance for many technologies involving flow separation on smoothly curved bodies.

Acknowledgements

The numerous technical discussions within the AVT-349 team are gratefully acknowledged. We also express special thanks to William Devenport and Holger Babinsky for their commendable leadership of the AVT-349 team.

Disclosure statement

No potential conflict of interest was reported by the author(s).

Funding

The DLR/UniBw experiment was funded by DFG (Grant KA 1808/14-1 & SCHR 1165/3-1), by the DLR institute of aerodynamics and flow technology, and by the DLR program directory board within the DLR internal projects VicToria and ADaMant. The authors from Virginia Tech would like to thank Dr. Peter Chang and Dr. Julie Young of the Office of Naval Research for their support under grant numbers N00014-18-1-2455, N00014-19-1-2109, and N00014-20-2821. Some of the research from the University of Melbourne and Stanford University was supported by the Office of Naval Research under grant N00014-17-1-2307, Dr. Peter Chang program lead. We would also acknowledge the U.S. Department of Defense High Performance Computing Modernisation Program (HPCMP) for computational support. The research by MARIN is partly funded by the Dutch Ministry of Economic Affairs.

Data availability statement

Available upon request.

ORCID

Volino Ralph  <http://orcid.org/0000-0003-1202-4029>

References

- [1] Devenport WJ, Lowe KT. Equilibrium and non-equilibrium turbulent boundary layers. *Prog Aerosp Sci.* 2022;131:100807. doi:10.1016/j.paerosci.2022.100807
- [2] Clauser FH. Turbulent boundary layers in adverse pressure gradients. *J Aeronaut Sci.* 1954;21:91–108. doi:10.2514/8.2938
- [3] Spalart P, Allmaras S. A one-equation turbulence model for aerodynamic flows. In *AIAA 30th Aerospace Sciences Meeting*. Reno NV, USA, 1992.
- [4] Menter FR. Two-equation eddy-viscosity turbulence models for engineering applications. *AIAA J.* 1994;32:1598–1605. doi:10.2514/3.12149

- [5] Eisfeld B, Rumsey C, Togiti V. Verification and validation of a second-moment closure model. *AIAA J.* 2016;54:1524–1541. doi:10.2514/1.J054718
- [6] Fritsch DJ, Vishwanathan V, Lowe KT, et al. Fluctuating pressure beneath smooth-wall boundary layers in non-equilibrium pressure gradients. *AIAA J.* 2022;60:4725–4743. doi:10.2514/1.J061431
- [7] Menter FR, Kuntz M, Langtry R, et al. Ten years of industrial experience with the SST turbulence model. In 4th Internal Symposium, Turbulence, Heat and Mass Transfer, 4, 625–632, Begell House, 2003.
- [8] Kok JC. Resolving the dependence on freestream values for the k-turbulence model. *AIAA J.* 2000;38:1292–1295.
- [9] Menter F, Egorov T, Rusch D. Steady and unsteady flow modelling using the model. in 5th Internal Symposium, Turbulence, Heat and Mass Transfer, 5, 403–406, Begell House, 2006.
- [10] Duraisamy K, Iaccarino G, Xiao H. Turbulence modeling in the age of data. *Ann Rev Fluid Mech.* 2019;51:357–377. doi:10.1146/annurev-fluid-010518-040547
- [11] Weatheritt J, Sandberg R. A novel evolutionary algorithm applied to algebraic modifications of the RANS stress-strain relationship. *J Comp Phys.* 2016;325:22–37. doi:10.1016/j.jcp.2016.08.015
- [12] Weatheritt J, Sandberg R. The development of algebraic stress models using a novel evolutionary algorithm. *Int J Heat Fluid Flow.* 2017;68:298–318. doi:10.1016/j.ijheatfluidflow.2017.09.017
- [13] Zhao Y, Akolekar HD, Weatheritt J, et al. RANS turbulence model development using CFD-driven machine learning. *J Comput Phys.* 2020;411:109413. doi:10.1016/j.jcp.2020.109413
- [14] Holland J, Baeder J, Duraisamy K. Towards integrated field inversion and machine learning with embedded neural networks for RANS modeling. *AIAA Scitech 2019 Forum.* 2019: 1884.
- [15] Vishwanathan V, Fritsch DJ, Lowe KT, et al. History effects and wall similarity of non-equilibrium turbulent boundary layers in varying pressure gradient over rough and smooth surfaces. *Int J Heat Fluid Flow.* 2023;102:109–145. doi:10.1016/j.ijheatfluidflow.2023.109145
- [16] Vishwanathan V. The Resolution and structure of high Reynolds number turbulent boundary layers over rough and smooth walls in pressure gradient. *Aerospace Ocean Eng. Virginia Tech. PhD.* 2023. <https://vtechworks.lib.vt.edu/handle/10919/113290>
- [17] Fritsch DJ. (2022). The effects of pressure gradient and roughness on pressure fluctuations beneath high Reynolds number boundary layers. *Aerospace and Ocean Engineering, Virginia Tech. PhD.* <https://vtechworks.lib.vt.edu/handle/10919/115587>.
- [18] Romero S, Zimmerman S, Philip J, et al. Properties of the inertial sublayer in adverse pressure gradient turbulent boundary layers. *J Fluid Mech.* 2022;937:A30. doi:10.1017/jfm.2022.6
- [19] Romero S, Zimmerman S, Philip J, et al. Velocity spectra and scale decomposition of adverse pressure gradient turbulent boundary layers. *Int J Heat and Fluid Flow.* 2023;102:109143. doi:10.1016/j.ijheatfluidflow.2023.109143
- [20] Volino RJ. Non-equilibrium development in turbulent boundary layers with changing pressure gradients. *J Fluid Mech.* 2020;897:A2. doi:10.1017/jfm.2020.319
- [21] Volino RJ, Schultz MP. Comparison of smooth- and rough-wall non-equilibrium boundary layers with favourable and adverse pressure gradients. *J Fluid Mech.* 2023;859:A35. doi:10.1017/jfm.2023.160
- [22] Knopp T, Reuther N, Novara M, et al. Experimental analysis of the log law at adverse pressure gradient. *J Fluid Mech.* 2021;918:A17-1–A17-32. doi:10.1017/jfm.2021.331
- [23] Knopp T, Schanz D, Novara M, et al. Experimental and numerical investigation of turbulent boundary layers with strong pressure gradients. *AIAA Paper.* 2022: 2022–1035. doi:10.2514/6.2022-1035.
- [24] Fritsch DJ, Vishwanathan V, Roy CJ, et al. Modeling the surface pressure spectrum beneath turbulent boundary layers in pressure gradients. *AIAA J.* 2023;61:2002–2021. doi:10.2514/1.J062074
- [25] Shubham S, et al. Data-driven empirical wall pressure spectrum models for fan noise prediction. *AIAA AVIATION.* 2023 Forum. 2023.
- [26] Eca L, Kerkvliet M, Toxopeus S. Simulation of 2D smooth-wall turbulent boundary layers with variable pressure gradient using RANS. *Tech. Rep. M-10, IST,* 2022.
- [27] Eca L, Dowding K, Roach PJ. On the interpretation and scope of the V&V 20 standard for verification and validation in computational fluid dynamics and heat transfer. *J Verif Valid and Uncert Quant.* 2022;7:021005.
- [28] Eca L, Kerkvliet M, Toxopeus S. On the numerical convergence properties of the calculation of the flow around the KVLCC2 tanker in unstructured grids. In 10th International Conference on Computational Methods in Marine Engineering, MARINE: June 2023.
- [29] Mellor GL, Gibson DM. Equilibrium turbulent boundary layers. *J Fluid Mech.* 1966;24:225–253. doi:10.1017/S0022112066000612
- [30] Romero S, Zimmerman S, Philip J, et al. Stress equation based scaling framework for adverse pressure gradient turbulent boundary layers. *Int J Heat Fluid Flow.* 2022;93:108885. doi:10.1016/j.ijheatfluidflow.2021.108885
- [31] Vishwanathan V, Fritsch DJ, Lowe KT, et al. History effects and wall similarity of non-equilibrium turbulent boundary layers in varying pressure gradient over rough and smooth surfaces, 12th International Symposium on Turbulence and Shear Flow Phenomena (TSFP12). Osaka, Japan; July 19-22, 2022.
- [32] McKeon BJ. The engine behind (wall) turbulence: perspectives on scale interactions. *J Fluid Mech.* 2017;817:P1. doi:10.1017/jfm.2017.115
- [33] Gomez SR. Linear amplification in nonequilibrium turbulent boundary layers. *PhD thesis, California Institute of Technology,* 2023.

- [34] Bobke A, Vinuesa R, Orlu R, et al. History effects and near equilibrium in adverse-pressure-gradient turbulent boundary layers. *J Fluid Mech.* 2017;820:667–692. doi:10.1017/jfm.2017.236
- [35] Pozuelo R, Li Q, Schlatter P, et al. An adverse-pressure-gradient turbulent boundary layer with nearly constant $\beta \simeq 1.4$ up to $Re_\theta \simeq 8700$. *J Fluid Mech.* 2022;939:A34. doi:10.1017/jfm.2022.221
- [36] Romero S, Zimmerman S, Philip J, et al. Detailing history and non-equilibrium effects in adverse pressure gradient turbulent boundary layers. *Progress in Turbulence X*. Springer-Verlag. 2024. doi:10.1007/978-3-031-55924-2
- [37] Knopp T, Reuther N, Novara M, et al. Modification of the SSG/LRR-omega model for adverse pressure gradients. *Flow Turb Combust.* 2022;409:438.
- [38] Nickels TB. Inner scaling for wall-bounded flows subject to large pressure gradients. *J Fluid Mech.* 2004;521:217–239. doi:10.1017/S0022112004001788
- [39] Townsend AA. The structure of turbulent shear flow. Cambridge University Press; Cambridge England; 1976.
- [40] Jones W, Launder B. The prediction of laminarization with a two-equation model of turbulence. *Int J Heat Mass Transf.* 1972;15:301–314. doi:10.1016/0017-9310(72)90076-2
- [41] Spalart PR. Numerical study of sink-flow boundary layers. *J Fluid Mech.* 1986;172:307–328. doi:10.1017/S0022112086001751
- [42] Yuan J, Piomelli U. Numerical simulations of sink-flow boundary layers over rough surfaces. *Phys Fluids.* 2014;26:015113. doi:10.1063/1.4862672
- [43] Wei T, Knopp T. Outer scaling of the mean momentum equation for turbulent boundary layers under adverse pressure gradient. *J Fluid Mech.* 2023;958:A9. doi:10.1017/jfm.2023.72
- [44] Fife P, Klewicki J, Wei T. Time averaging in turbulence settings may reveal an infinite hierarchy of length scales. *Discret Contin Dyn Sys A.* 2009;24:781. doi:10.3934/dcds.2009.24.781
- [45] Skare PE, Krogstad PA. A turbulent equilibrium boundary layer near separation. *J Fluid Mech.* 1994;272:319–348. doi:10.1017/S0022112094004489
- [46] Sporschill G. Improved Reynolds-stress modeling for adverse-pressure-gradient turbulent boundary layers in industrial aeronautical flow. France: Universite de Pau et des Pays de l'Adour; 2021.
- [47] Zimmerman SJ. Experimental investigation of velocity and vorticity in turbulent wall flows. PhD Thesis, 2019, University of Melbourne.
- [48] Schlatter P, Orlu R. Assessment of direct numerical simulation data of turbulent boundary layers. *J Fluid Mech.* 2010;659:116–126. doi:10.1017/S0022112010003113
- [49] Eca L, Kerkvliet M, Toxopeus S. Comparison of RANS turbulence models for the simulation of smooth Wall boundary-layers in pressure gradients at moderate and high Reynolds numbers. In *Proceedings of the Tenth International Conference on Computational Methods in Marine Engineering (MARINE)*. June, 2023.